Robotica (2013) volume 31, pp. 99–112. © Cambridge University Press 2012
doi:10.1017/S0263574712000124

A novel line of sight control system for a robot vision tracking system, using vision feedback and motion-disturbance feedforward compensation

Jaehong Park, Wonsang Hwang†, Hyunil Kwon‡, Kwangsoo Kim§, and Dong-il "Dan" Cho¶*

†*LG Display Co., LTD, Gumi, 730-726, Korea*
‡*Multimedia R & D Lab., LG Electronics Inc., Seocho-gu, Seoul, 137-130, Korea*
§*Department of Control and Instrumentation Engineering, Hanbat National University, Yuseong-gu, Deajeon, 305-719, Korea*
¶*ASRI/ISRC/Department of Electrical Engineering and Computer Science, Seoul National University, Kwanak-ku, Seoul, 151-742, Korea*

(Accepted March 9, 2012. First published online: April 12, 2012)

SUMMARY
This paper presents a novel line of sight control system for a robot vision tracking system, which uses a position feedforward controller to preposition a camera, and a vision feedback controller to compensate for the positioning error. Continuous target tracking is an important function for service robots, surveillance robots, and cooperating robot systems. However, it is difficult to track a specific target using only vision information, while a robot is in motion. This is especially true when a robot is moving fast or rotating fast. The proposed system controls the camera line of sight, using a feedforward controller based on estimated robot position and motion information. Specifically, the camera is rotated in the direction opposite to the motion of the robot. To implement the system, a disturbance compensator is developed to determine the current position of the robot, even when the robot wheels slip. The disturbance compensator is comprised of two extended Kalman filters (EKFs) and a slip detector. The inputs of the disturbance compensator are data from an accelerometer, a gyroscope, and two wheel-encoders. The vision feedback information, which is the targeting error, is used as the measurement update for the two EKFs. Using output of the disturbance compensator, an actuation module pans the camera to locate a target at the center of an image plane. This line of sight control methodology improves the recognition performance of the vision tracking system, by keeping a target image at the center of an image frame. The proposed system is implemented on a two-wheeled robot. Experiments are performed for various robot motion scenarios in dynamic situations to evaluate the tracking and recognition performance. Experimental results showed the proposed system achieves high tracking and recognition performances with a small targeting error.

KEYWORDS: Line of sight control system; Vision tracking system; Feedforward controller; Feedback controller; Disturbance compensator; Extended kalman filter; Slip detector.

* Corresponding author. E-mail: dicho@snu.ac.kr

1. Introduction

The performance of robots is highly dependent on their sensing ability. Vision systems are especially crucial to recognize and acquire information about the surroundings.[1,2] Vision systems are most commonly used for target tracking, target recognition, surrounding perception, localization, navigation, and attitude estimation in robots, and the target tracking function has emerged as an important function for Human Robot Interaction (HRI). That is, a continuous monitoring function of the target based on vision tracking is of a great importance for HRI. The vision tracking system is divided into four categories based on the states of the camera or robot and its environment: (1) Stationary Camera, Stationary Object (SCSO), (2) Stationary Camera, Moving Object (SCMO), (3) Moving Camera, Stationary Object (MCSO), (4) Moving Camera, Moving Object (MCMO), as shown in Fig. 1.[3] In the case of a mobile robot, since the camera integrated with the mobile robot is moving, the MCSO and MCMO states are considered.[4] The vision tracking can be realized by the vision-based system. However, it is difficult to continuously acquire vision information due to changes in environmental conditions, image blurring, and the temporary absence of vision information.[5] In addition, as the demands for the high performance system have increased, heavy and complicated image-processing algorithms are required. Especially, when a robot is moving fast, a vision-based system cannot fix the camera's sight to the specific target. To overcome this difficulty, a novel vision tracking systems based on sensor fusion methods and biomimetic concepts have been investigated by many researchers. The detailed reviews of the previous researches are described in Section 2.

In this paper, a novel line of sight control system for a robot vision tracking system by a position feedforward controller

https://doi.org/10.1017/S0263574712000124 Published online by Cambridge University Press

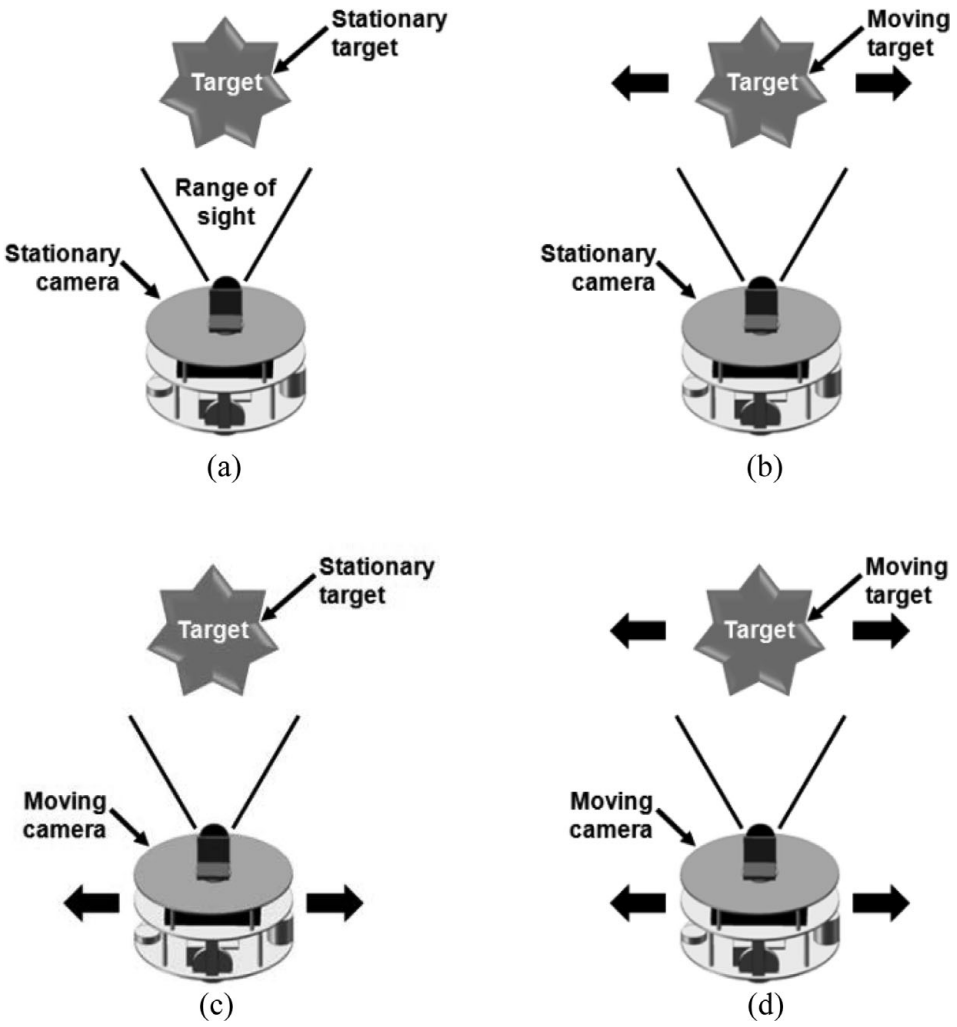


Fig. 1. Four categories of the vision tracking system[2]. (a) Stationary Camera, Stationary Object (SCSO) (b) Stationary Camera, Moving Object (SCMO) (c) Moving Camera, Stationary Object (MCSO) (d) Moving Camera, Moving Object (MCMO).

and a vision feedback controller is presented. This concept is similar function to the human eye reflex mechanisms. The main purpose of the proposed system is to keep the camera's line of sight fixed on the stationary target even when the robot has large and continuous transient movements. The proposed control system belongs to the third category of the vision tracking systems, as shown in Fig. 1(c). It is applied to various robot applications, including service, human-robot cooperation, and military applications. In this paper, the main application of the proposed system is indoor robots, which typically moves on a plane. The feedforward controller is realized based on the inertial sensor data and the wheel-encoder data to preposition the camera to track the specified target, even in the wheel-slip condition. A disturbance compensator produces the feedforward control signal based on estimated robot position and motion information. The disturbance compensator consists of two extended Kalman filters (EKFs) and a slip detector. The vision feedback information is used as the measurement update information to compensate for the tracking error.

This remainder of this paper is organized as follows. Section 2 reviews the state of the art. Section 3 describes the concept of proposed system. Section 4 describes signal processing methods for the motion information and the visual information. Section 5 shows the coordinate systems that are used for the proposed system. Section 6 briefly explains the disturbance compensator. Sections 7 and 8 show the implementation and experimental results of the developed system, respectively. Finally, we discuss the significance of our findings and conclude this paper in Section 9.

2. The State of the Art

The previous vision tracking systems can be categorized into the following three categories, vision-only-based systems, motion-information-based systems, and biomimetic systems. First, vision-only-based systems have been developed by many research groups.[6–9] Kragić discussed visual cue integration methods for the visual servoing and tracking system.[6] The methods are based on weak or model-free approaches to integration. Cai and Nillius presented vision-based tracking systems for multiple targets using particle filter and Bayesian network.[7,8] Jung developed a detection system for a moving target using a single camera on a mobile robot.[9] These systems require complex algorithms for vision processing and filtering, regardless of background

https://doi.org/10.1017/S0263574712000124 Published online by Cambridge University Press

clutter and camera motion. Therefore, vision-only-based systems generally have a large time delay due to the heavy computation requirements. In addition, these systems do not function well in the absence of the vision information. In practice, when an object is hidden behind an obstacle or illumination is changed, the vision information of the object is not generated sufficiently for target tracking.

Second, motion-information-based systems have also been presented by several research groups.[10–15] These systems used inertial sensors to compute the motion information of the camera. Dai compensated for perturbations of the camera using a 3-axis gyroscope.[10] Hwangbo developed the inertial-aided Kanade–Lucas–Tomasi (KLT) feature tracking method using gyroscope data.[11] Jia proposed the data fusion scheme for visual object identification and tracking by autonomous vehicles.[12] Ribo showed the hybrid tracking method using an inertial sensor and vision sensor fusion.[13] Xu proposed the sensing system with inertial and active vision sensors using the hierarchical fusion strategy.[14] The major purpose of these systems focused on the camera stabilization and compensation for small rotation motion or tracking a target in the image frame using self-motion information. Lobo's system used the rotational motion and linear motion of a camera from the gyroscope data and the accelerometer data.[15] However, the main purpose of this system involved the camera attitude estimation, the motion estimation, and the 3-dimensional structure reconstruction.

Third, biomimetic systems were recently developed by some research groups.[16–19] Shibata, Xie, Lenz, and Ouh presented biomimetic vision stabilization systems for mobile robot applications.[16–19] Shibata's systems used a Vestibulo-Ocular Reflex (VOR) and an Opto-Kinetic Reflex (OKR), which are the human eye reflexes, to improve the performance of the vision system.[16] Xie developed the biomimetic control of a pan-tilt camera for visual tracking based-on an autonomous helicopter.[17] Lenz also developed an adaptive gaze stabilization controller inspired by the VOR.[18] The main purpose of these systems is to realize the vision stabilization for small rotation motion and vibration, rather than to track a specified target. Ouh presented the VOR based target tracking system using accelerometer information.[19] Ouh's vision system focused on the tracking function for translational robot motion. The camera, mounted on the robot, rotates toward the selected target, periodically compensating errors from visual information from the accelerometer information for the translational motion.

As mentioned above, previous vision tracking systems have disadvantages and limitations as follows. First, the vision-only-based systems do not function well when the update time is slow due to computational requirements, or when occlusion is present. They also do not function well when lighting condition is poor, or when vibration-induced blurring takes place. Second, most of motion-information-based vision systems and biomimetic vision systems developed to date are focused on vision system stabilization for compensation of local and small rotation or movements of the camera. The proposed vision tracking system is designed to track an object while a mobile robot is performing its normal motion, which is much larger than camera vibration. The proposed system uses the robot motion information, which is computed using inertial sensors and wheel encoders in a feedforward control signal to preposition the camera toward a target, and the vision information as a feedback control signal to position a target image in the center of an image frame.

3. Concept of the Proposed Line of Sight Control System

3.1. Human eye reflex mechanisms

The human eye reflex comprises the VOR and the OKR. The VOR is feedforward control using head motion information. The OKR is feedback control using the visual information. During locomotion, the head oscillates passively on the trunk and the images of the visual surroundings tend to smear across the retina. Image motion is minimized and visual perception is facilitated by the initiation of eye movements in the opposite direction to the head movement. The VOR generates these compensatory eye movements. Horizontal and vertical, angular and linear head movement components activate the appropriate combinations of extraocular muscles via short reflex pathways. The VOR acts rapidly – the eyes start to move 10–20 ms after the onset of a head movement. However, they need to be supplemented by visual information due to the absence of a feedback signal from the eyes. A leftward passive head movement generates both compensatory the VOR to the right and the OKR that makes the eye follow the apparent image motion to the right. Both reflexes are therefore activated simultaneously, generate eye movements in the same direction, but differ in their dynamic properties. OKRs are about 10 times slower in their onset and are best tuned to low frequencies of head movements (50–5 Hz), whereas VORs are best tuned to higher frequencies of head movements (0.5–5 Hz).[16,20]

3.2. Proposed line of sight control system

The block diagram of the proposed line of sight control system is shown in Fig. 2. The basic concept of the proposed system is similar to the human eye reflex mechanisms. Adding similar functions of the human eye reflex mechanisms to the robot vision system, a target is fixed on the center of the vision sensor under dynamic conditions. This mechanism improves the tracking stability and recognition performance of the vision tracking system. The simple control procedure of the proposed system is summarized as follows. When the robot starts to move based on the robot trajectory input, the robot motion information is generated by inertial sensors and wheel encoders. The inertial sensor data and the wheel-encoder data are introduced to the disturbance compensator to determine the current robot position. The disturbance compensator generates the expected rotation angle of the camera based on the estimated robot position relative to the target. The multisensor data fusion is achieved using two EKFs and the slip detector in the disturbance compensator. The output of the disturbance compensator, which is the feedforward control signal, is the fed to the command generator. In the command generator, the motor control signal is generated using the feedforward signal. Then, the pan motor controls the camera's line of

https://doi.org/10.1017/S0263574712000124 Published online by Cambridge University Press

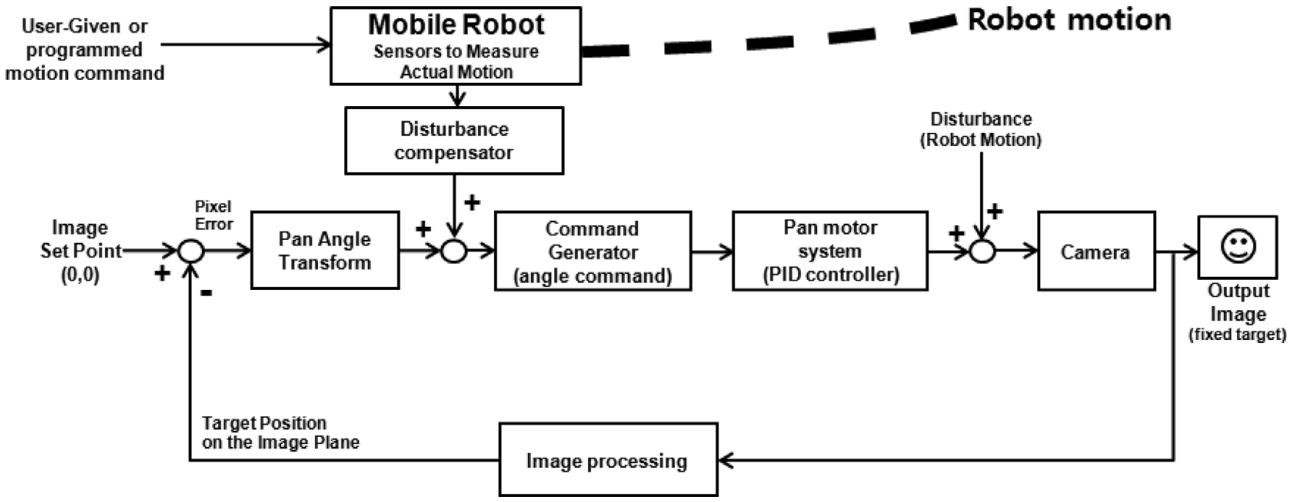


Fig. 2. Block diagram of the proposed line of sight control system.

sight, and the target image is fixed in the center of the image frame during locomotion. The pan motor system has a built-in Proportional–Integral–Derivative (PID) controller, as shown in Fig. 2. Consequently, the tracking and recognition success rates are improvable, while the robot is moving, due to the fixation of the target in the image plane. Additionally, a targeting error, which is produced by the image processing and the pan angle transform block, is used to compensate for the tracking error due to the estimation error.

As mentioned in Section 2, the vision-based system is unable to be applied in dynamic circumstances due to the significant delay from the large computation time. Thus, when the robot moves in fast motion, these systems are unable to track the target successfully. In addition, the vision-based system does not function well in the absence of visual information. In practice, when object is hidden behind an obstacle or illumination is changed, vision information of the object is insufficiently generated and is unstable. On the other hand, in the case of the robot position information based system, it is possible to track the target even in fast robot motion, using the motion sensors. However, the position information based system is unable to track the target for a long time due to sensor error accumulation. The proposed vision tracking system is able to improve the tracking performance, using both position information and vision information. This feature is similar to the previous vision tracking system based on sensor fusion methods and biomimetic concepts. However, most of the previous researches are focused on the camera stabilization and the small motion compensation. The main purpose of the proposed system is to track the target even when the robot has large and continuous transient movements.

4. Motion and Vision Information for Line of Sight Control System

4.1. Motion information

The motion information for robot position estimation is obtained by an accelerometer, a gyroscope, and two wheel-encoders. The robot position, including heading angle information, can be estimated using the inertial sensors under unexpected circumstances including the wheel-slip conditions. However, the position estimation using inertial sensors is reliable over only short periods due to the accumulation of systematic and random errors.[21] Especially, errors of the accelerometer cause an unbounded growth through twice-integrated measurements. Thus, the motion information from the inertial sensors is initialized when the robot is stopped to reduce accumulation of these errors. Additionally, an averaging algorithm and a low-pass filter are used to obtain a relatively smooth shape for the inertial sensor signal without damaging the integral value of the original signal.[22] A standard third-order Chebyshev II low-pass filter is developed to eliminate the high frequency noise of the accelerometer data due to the external vibration.[23] The simple block diagram for the inertial sensor signal processing is shown in Fig. 3.

The wheel-encoder data represent the rotation angle of the wheel motor. Using this information, the moving distance and rotation angle of the robot can be calculated[21] The wheel-encoder data are more accurate than the inertial sensor data. However, the motion information from the wheel-encoders is unreliable under wheel slip conditions. Two EKFs and the slip detector are implemented in the disturbance compensator to overcome the drawbacks of the inertial sensor data and the wheel-encoder data. The detailed descriptions of sensor fusion method are explained in Section 5.

4.2. Vision feedback information

The vision data are the targeting angle error of the camera position from the image-processing block and angle error calculation block. This information is the feedback data for the controller, as shown in Fig. 2. The targeting angle error is calculated using the pixel error between the center of the image plane of the camera and the center of the target in the image plane. The camera angle error is calculated using the pin-hole model.[24] The angle error is shown in Eq. (1), and the pin-hole model is shown in Fig. 4.

$$\varepsilon_k = \tan^{-1}\left(\frac{\mathrm{d}}{\mathrm{l}}\right), \tag{1}$$

https://doi.org/10.1017/S0263574712000124 Published online by Cambridge University Press

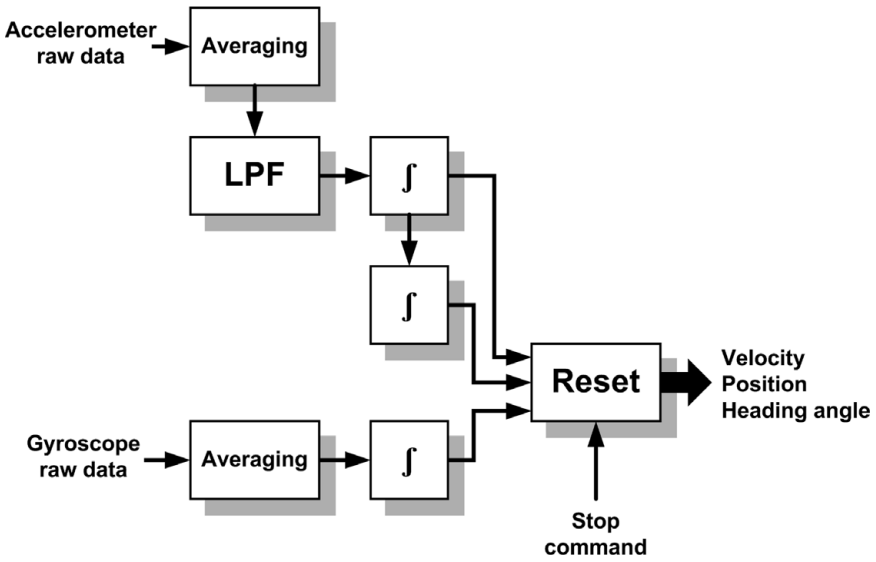


Fig. 3. Structure for the inertial sensor signal processing.

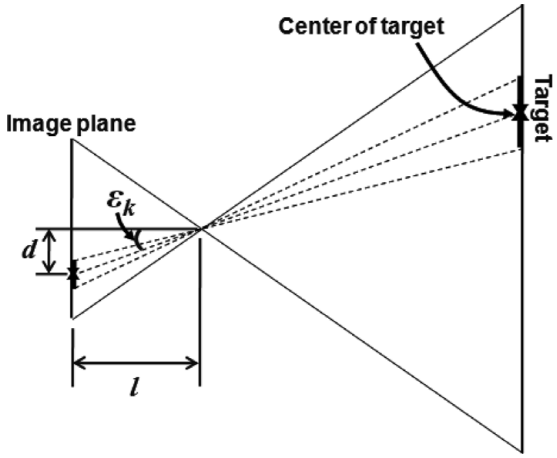


Fig. 4. Schematic diagram of the pin-hole model to calculate camera angle error.

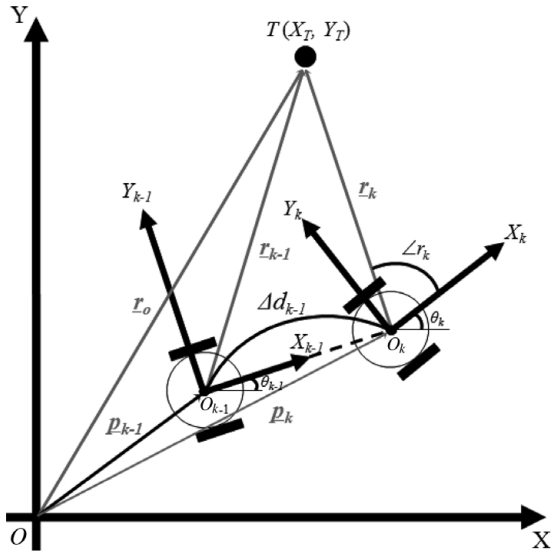


Fig. 5. Cartesian coordinate system for the proposed vision tracking system.

where ε_k is the angle error from image processing, d is the distance from the image center to target center, and l is the camera focal length. Considering the computational load, the Speeded Up Robust Features (SURF) algorithm is used to recognize the target and compute the target position in the image plane.[25] Only horizontal error information is used to compensate for the targeting angle error, because only the pan motion is required to track the target while the robot moves in a plane.

5. Coordinate System

The proposed line of sight control system is developed for the vision tracking system, which is implemented on a two-wheeled robot for indoor applications. The two-wheeled robot has in-plane motion with three degrees of freedom. These contain linear motions in x/y-axis and rotation motions in z-axis. Considering these motions, we applied Cartesian coordinate system to express the robot motion and position, as shown in Fig. 5.[26,27] There are two coordinate systems: global coordinate (centered at O) and intermediate coordinate system (centered at O_k), as shown in Fig 2. In this coordinate system, r_k, vector from robot to target, can be expressed as

$$\underline{r}_k = \underline{r}_o - \underline{p}_k, \tag{2}$$

where, $\underline{r}_0$ is the vector from origin to target, $T(X_T, Y_T)$ is the target position in the global coordinate, and $\underline{p}_k$ is the robot location vector. According to present coordinate system, $\underline{r}_k$ can be expressed as

$$\underline{r}_k = \begin{bmatrix} \cos\theta_k & \sin\theta_k \\ -\sin\theta_k & \cos\theta_k \end{bmatrix} \cdot (\underline{r}_o - \underline{p}_k), \tag{3}$$

where θ_k is the robot heading angle with respect to the initial coordinate system. Using Eqs. (2) and (3), the expected

https://doi.org/10.1017/S0263574712000124 Published online by Cambridge University Press

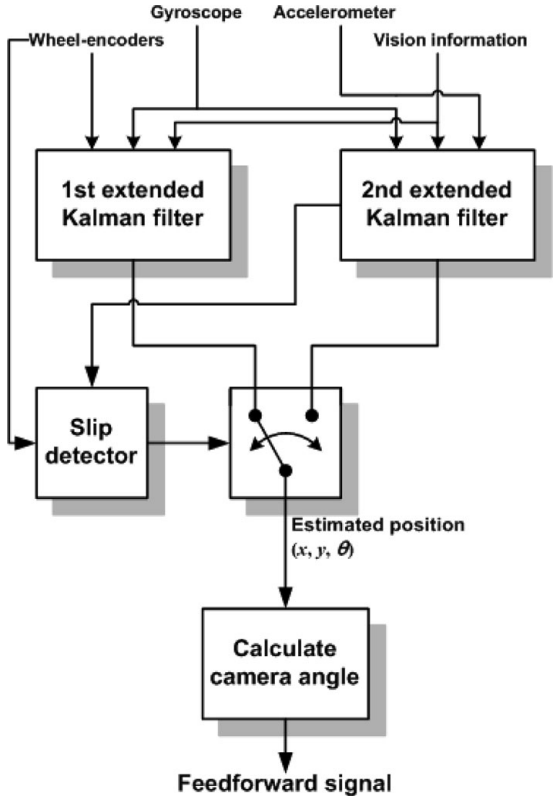


Fig. 6. Block diagram of the disturbance compensator.

camera rotation angle, $\angle r_k$, is calculated by

$$\begin{aligned}\angle r_k &= \tan^{-1}\left(\frac{r_{y,k}}{r_{x,k}}\right)\\ &= \tan^{-1}\left(\frac{-(X-p_{x,k})\cdot\sin\theta_k+(Y-p_{y,k})\cos\theta_k}{(X-p_{x,k})\cos\theta_k+(Y-p_{y,k})\sin\theta_k}\right).\end{aligned} \tag{4}$$

6. Sensor Fusion Method of Disturbance Compensator

The multisensor fusion to estimate the robot position is performed in the disturbance compensator. Using the estimation results, the feedforward control signal, which is the expected rotation angle of the camera, is calculated by using Eq. (4). The accelerometer data, the gyroscope data, the wheel-encoder data, and the vision feedback data are the inputs of the disturbance compensator. The wheel-encoders can provide accurate robot position, but the encoder data are unreliable on the slippery floor. The robot position information from the accelerometer data is reliable on slippery or rugged roads with wheel-slip. However, the short-term position estimation is reliable due to the integration of errors arising from bias and noise.[21,28] The proposed disturbance compensator includes the two EKFs and the slip detector to overcome disadvantages of the each sensor system, as shown in Fig. 6. The first EKF is based on the data from wheel-encoders and the gyroscope. This filter is used when wheel-slip is not detected. The other EKF uses the data from the accelerometer and the gyroscope. This second filter

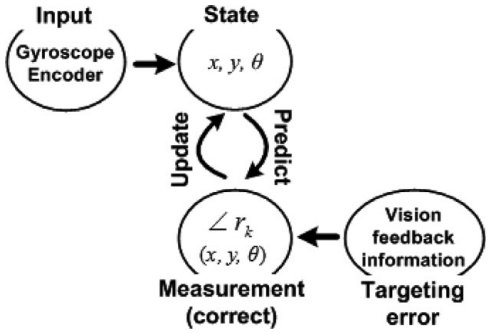


Fig. 7. Schematic diagram of the first extended Kalman filter for the nonslip condition.

is used when wheel-slip is detected, where the encoder data are erroneous. The position estimation using the Unscented Kalman Filter (UKF) and the Particle Filter (PF) is more accurate than the EKF results. However, the UKF and the PF require high computational load for position estimation.[29,30] The robot position information is used to calculate the camera rotation angle in the proposed vision tracking system. Thus, the accuracy of the position estimation is not crucial to the navigation system and localization system.[31,32] In addition, the EKF is implemented for the proposed system, to consider real-time control and to reduce the computational load. The slip detector compares the velocity data from the accelerometer and the wheel-encoders, and decides if a slip condition has occurred. Accordingly, based on the decision of the slip detector, the system chooses one of the outputs of two Kalman filters. This is subsequently used to calculate the rotation angle of the camera.

6.1. First EFK for nonslip condition

The schematic diagram of the first EKF for the nonslip condition is shown in Fig. 7. In the nonslip condition, the encoder data provide accurate robot position information. The vision feedback data are used as the measurement value in this filter. The state of the Kalman filter is shown in Eq. (5).

$$\underline{x} = \begin{bmatrix} x & y & \theta \end{bmatrix}^T, \tag{5}$$

where x, y, and θ are the position in the x-direction and the y-direction, and the attitude angle of robot, respectively. The state model is derived in Eqs. (6) and (7).

$$\hat{\underline{x}}_{k+1} = f(\hat{\underline{x}}_k, u_k, \underline{w}_k) = \begin{bmatrix} \hat{x}_k + \sin\hat{\theta}_k \cdot \frac{(d_k^R+\varepsilon_e^R)+(d_k^L+\varepsilon_e^L)}{2} \\ \hat{y}_k + \cos\hat{\theta}_k \cdot \frac{(d_k^R+\varepsilon_e^R)+(d_k^L+\varepsilon_e^L)}{2} \\ \hat{\theta}_k + (\omega_k+\varepsilon_g)\cdot\Delta t \end{bmatrix}, \tag{6}$$

$$w_k = \begin{bmatrix} \frac{\sin\hat{\theta}_k}{2} & \frac{\sin\hat{\theta}_k}{2} & 0 \\ \frac{\cos\hat{\theta}_k}{2} & \frac{\cos\hat{\theta}_k}{2} & 0 \\ 0 & 0 & \Delta t \end{bmatrix} \begin{bmatrix} \varepsilon_e^R \\ \varepsilon_e^L \\ \varepsilon_g \end{bmatrix}, \tag{7}$$

https://doi.org/10.1017/S0263574712000124 Published online by Cambridge University Press

where $f(\cdot)$ is the system equation, $\hat{x}$, $\hat{y}$, and $\hat{\theta}$ are the estimates of the states, u_k is the input of the Kalman filter, w_k is the process noise added by the sensor noise, $d_k^R + \varepsilon_e^R$ is the output of the right wheel-encoder with true value (d_k^R) and noise (ε_e^R), $d_k^L + \varepsilon_e^L$ is the output of the right wheel-encoder with true value (d_k^L) and noise (ε_e^L), $\omega_k + \varepsilon_g$ is the output of the gyroscope with true value (ω_k) and noise (ε_g), and Δt is the sampling time. The wheel-encoder data are used as the input to give this filter the position and the velocity of the robot. The gyroscope data are used to calculate the heading angle of the robot. The encoder data can also provide the information about the heading angle of the robot. However, the encoder data are not used to estimate the robot-heading angle in this system. If the gyroscope and the wheel-encoder are used together, the angular slip makes the system to choose the second EKF. This means that position estimation is performed with the accelerometer-based Kalman filter, even in the angular slip condition. In order to prevent the above case, the first EKF does not use the encoder to estimate the robot-heading angle. Thus, the slip detector in this system does not need to detect the angular slip.

The partial matrix for the covariance update is shown in Eq. (8)

$$F_{k+1} = \left.\frac{\partial f}{\partial \underset{\sim}{x}}\right|_{\underset{\sim}{x}=\hat{\underset{\sim}{x}}_k} = \begin{bmatrix} 1 & 0 & \cos\hat{\theta}_k \cdot \dfrac{d_k^R + d_k^L}{2} \\ 0 & 1 & -\sin\hat{\theta}_k \cdot \dfrac{d_k^R + d_k^L}{2} \\ 0 & 0 & 1 \end{bmatrix}, \quad (8)$$

where F_k is the partial derivate matrix of the state transition function. The error covariance estimate in the time update of first EKF is shown in Eq. (9).

$$P_{k+1} = F_k P_k F_k^T + L_k Q_k L_k^T, \quad (9)$$

$$L_k = \begin{bmatrix} \dfrac{\sin\hat{\theta}_k}{2} & \dfrac{\sin\hat{\theta}_k}{2} & 0 \\ \dfrac{\cos\hat{\theta}_k}{2} & \dfrac{\cos\hat{\theta}_k}{2} & 0 \\ 0 & 0 & \Delta t \end{bmatrix}, \quad (10)$$

$$Q_k = \begin{bmatrix} q\varepsilon_e^R & 0 & 0 \\ 0 & q\varepsilon_e^L & 0 \\ 0 & 0 & q\varepsilon_g \end{bmatrix}, \quad (11)$$

where P_k is the error covariance matrix, L_k is the first term of Eq. (9), and Q_k is the covariance matrix of the second term of Eq. (10). Using vision feedback data, the measurement update is performed to compensate for the estimation with the wheel-encoder and gyroscope. The measurement equation is derived in Eq. (12)

$$z_k = h_k(\hat{\underset{\sim}{x}}_k^-, v_k) = \tan^{-1}\left(\frac{Y_T - \hat{y}_k^-}{X_T - \hat{x}_k^-}\right) - \hat{\theta}_k^- + v_k, \quad (12)$$

where h_k is the measurement equation, $\hat{x}_k^-$, $\hat{y}_k^-$, $\hat{\theta}_k^-$ are the priori estimates of the states, X_T and Y_T are the position of the target, and v_k is the measurement noise. In this equation, z is the targeting error added by the actuation angle of the camera. The right side of Eq. (12) is the calculated result of the targeting error using the state value. The estimated state from feedforward input is corrected by feedback input via the measurement update. The partial matrices for estimating error covariance are shown in Eq. (13).

$$\begin{aligned} H_k &= \frac{\partial h_k}{\partial \hat{\underset{\sim}{x}}_k^-} \\ &= \left[\frac{Y_T - \hat{y}_k^-}{(X_T - \hat{x}_k^-)^2 + (Y_T - \hat{y}_k^-)^2} \quad \frac{X_T - \hat{x}_k^-}{(X_T - \hat{x}_k^-)^2 + (Y_T - \hat{y}_k^-)^2} \quad -1\right], \\ M_k &= \frac{\partial h_k}{\partial v_k} = [1], \end{aligned} \quad (13)$$

where H_k is the partial derivative of the measurement function with respect to the priori estimate, and M_k is the partial derivative of the measurement function with respect to the measurement noise. The equations for the Kalman gain, the posteriori state estimate, and the error covariance estimate are shown in Eq. (14).

$$\begin{aligned} K_k &= P_k^- H_k^T (H_k P_k^- H_k^T + M_k R_k M_k^T)^{-1} \\ \hat{\underset{\sim}{x}}_k^+ &= \hat{\underset{\sim}{x}}^- + K_k[z_k - h_k(\hat{\underset{\sim}{x}}_k^-, 0)] \\ P_k^+ &= (I - K_k H_k) P_k^-, \end{aligned} \quad (14)$$

where K_k is the Kalman gain, $\hat{x}_k^+$ is the posteriori estimate of the state, R_k is the covariance of the measurement noise, I is the identity matrix, P_k^+ is the posteriori estimate of the error covariance of the state, and P_k^- is the priori estimate.

6.2. Second EKF for slip condition

The schematic diagram of the second EKF for slip condition is shown in Fig. 8. The inertial sensor data are used for the input of the Kalman filter. The vision feedback data are also used for the measurement value. The state of the Kalman filter is given in Eq. (15).

$$\underset{\sim}{x} = \begin{bmatrix} x & y & v & \theta \end{bmatrix}^T, \quad (15)$$

where x, y are the position of the robot, v is the robot velocity from the accelerometer data, and θ is the attitude angle of

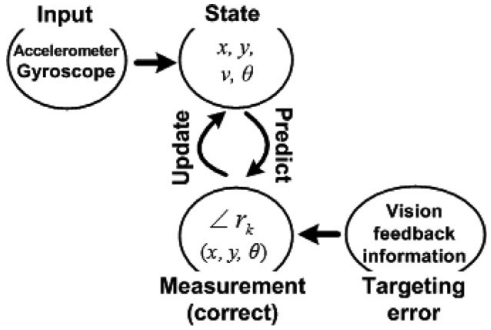


Fig. 8. Schematic diagram of the second extended Kalman filter for the slip condition.

https://doi.org/10.1017/S0263574712000124 Published online by Cambridge University Press

the robot. The state model is shown in Eq. (16).

$$\hat{\underline{x}}_{k+1} = f(\hat{\underline{x}}_k, u_k, \underline{w}_k) = \begin{bmatrix} \hat{x}_k + \hat{v}_k \cdot \cos\hat{\theta}_k \cdot \Delta t \\ \hat{y}_k + \hat{v}_k \cdot \sin\hat{\theta}_k \cdot \Delta t \\ \hat{v}_k + (a_k + \varepsilon_a) \cdot \Delta t \\ \hat{\theta}_k + (\omega_k + \varepsilon_g) \cdot \Delta t \end{bmatrix}, \quad (16)$$

where $f(\cdot)$ is the system equation, $\hat{x}$, $\hat{y}$, $\hat{v}$, and $\hat{\theta}$ are the estimates of the states, u_k is the input of the Kalman filter, $w_k = [0\ 0\ \varepsilon_a \cdot \Delta t\ \varepsilon_g \cdot \Delta t\ ]^T$ is the process noise added by the sensor noise, $a_k + \varepsilon_k$ is the acceleration data from the accelerometer with true value (a_k) and noise (ε_k), $\omega_k + \varepsilon_g$ is the output of the gyroscope with true value (ω_k) and noise (ε_g), and Δt is the sampling time. The velocity can be found by accumulating the acceleration value. In the same way, the heading angle of the robot can be found by accumulating the angular velocity value. The attitude angle decides the direction of the robot velocity. Therefore, the position is decided by Eq. (16).

The partial matrix for the covariance update is shown in Eq. (17).

$$F_k = \left.\frac{\partial \underline{f}}{\partial \underline{x}}\right|_{\underline{x}=\hat{\underline{x}}_k} = \begin{bmatrix} 1 & 0 & \cos\hat{\theta}_k \cdot \Delta t & -\hat{v}_k \cdot \sin\hat{\theta}_k \cdot \Delta t \\ 0 & 1 & -\sin\hat{\theta}_k \cdot \Delta t & \hat{v}_k \cdot \cos\hat{\theta}_k \cdot \Delta t \\ 0 & 0 & 1 & 0 \\ 0 & 0 & 0 & 1 \end{bmatrix}, \quad (17)$$

where F_k is the partial derivate matrix of the state transition function. The error covariance update equation and covariance matrix of the noise are shown in Eqs. (18) and (19).

$$P_{k+1} = F_k P_k F_k^T + Q_k, \quad (18)$$

$$Q_k = \begin{bmatrix} 0 & 0 & 0 & 0 \\ 0 & 0 & 0 & 0 \\ 0 & 0 & q \cdot \varepsilon_a \cdot \Delta t^2 & 0 \\ 0 & 0 & 0 & q \cdot \varepsilon_g \cdot \Delta t^2 \end{bmatrix}, \quad (19)$$

where P_k is the error covariance matrix, and Q_k is the covariance matrix of the noise. The inertial sensor noises are considered in the covariance matrix, because the sensor noise is much larger than the process noise of the Kalman filter. The measurement update is performed using vision feedback data to correct the estimation results with the accelerometer and gyroscope. The equations for measurement update in the second EKF are derived in Eqs. (20)–(22).

$$z_k = h_k(\hat{\underline{x}}_k^-, v_k) = \tan^{-1}\left(\frac{Y_T - \hat{y}_k^-}{X_T - \hat{x}_k^-}\right) - \hat{\theta}_k^- + v_k, \quad (20)$$

$$H_k = \frac{\partial h_k}{\partial \hat{\underline{x}}_k^-} = \begin{bmatrix} \frac{Y_T - \hat{y}_k^-}{(X_T - \hat{x}_k^-)^2 + (Y_T - \hat{y}_k^-)^2} & \frac{X_T - \hat{x}_k^-}{(X_T - \hat{x}_k^-)^2 + (Y_T - \hat{y}_k^-)^2} & -1 \end{bmatrix}$$

$$M_k = \frac{\partial h_k}{\partial v_k} = [1], \quad (21)$$

$$\begin{aligned} K_k &= P_k^- H_k^T (H_k P_k^- H_k^T + M_k R_k M_k^T)^{-1} \\ \hat{\underline{x}}_k^+ &= \hat{\underline{x}}^- + K_k[z_k - h_k(\hat{\underline{x}}_k^-, 0)] \\ P_k^+ &= (I - K_k H_k) P_k^-, \end{aligned} \quad (22)$$

where h_k is the measurement equation, $\hat{x}_k^-$, $\hat{y}_k^-$, $\hat{\theta}_k^-$ are the priori estimates of the states, X_T and Y_T are the positions of the target, v_k is the measurement noise, H_k is the partial derivative of the measurement function with respect to the priori estimate at time k, M_k is the partial derivative of the measurement function with respect to the measurement noise, K_k is the Kalman gain, $\hat{x}_k^+$ is the posteriori estimate of the state, R_k is the covariance of the measurement noise, I is the identity matrix, P_k^+ is the posteriori estimate of the error covariance of the state, and P_k^- is the priori estimate.

6.3. Slip detector

The slip detector decides the slip condition and makes the proposed system to choose one of the two EKF outputs. The concept to detect the translational slip is implemented using Seyr's method[33] The slip detector can decide the slip condition, comparing the calculated velocities from the accelerometer and the wheel-encoders. If the difference of two velocities exceeds the larger than threshold level, the slip detector decides that a slip condition has occured. The proposed system uses only the gyroscope to calculate the attitude angle. Therefore, the slip detector does not consider an angular slip. The condition to determine if the slip condition occurs is shown in Eq. (23).

$$|v_{encoder}(k) - v_{accel}(k)| > threshold, \quad (23)$$

where $v_{encoder}$ is the velocity estimation using the wheel-encoder data and v_{accel} is the velocity estimation using the accelerometer data. The threshold is determined by repetitive experiments. In this system, the threshold is chosen to be 0.07 m/s.

7. Vision Tracking System Implementation

The schematic diagram of the vision tracking system implemented the proposed line of sight control system is shown in Fig. 9. The proposed system consists of an accelerometer, gyroscope, camera, DC motor to rotate the camera, and host computer. The robot motion information, such as the acceleration, the angular velocity, and the wheel-encoder data, are transferred from sensors to the host computer by using a RS232 interface. The vision signal and motor control signal are transferred by using an USB interface.

A sensor module is developed as shown in Fig. 10(a), to process the inertial sensors data and the wheel-encoder data simultaneously. The sensor module, which detects the rotational and translational motions of the robot, functions in a similar manner as the semicircular canals and otoliths in human vestibular system. The sensor module contains an accelerometer (KXPS5–3157, Kionix, Inc.), gyroscope (ADIS16255, Analog Devices, Inc.), micro controller unit (MCU), and RS232 chip. The pan motion actuation module with camera is developed as shown in Fig. 10(b). The panning motion for the wheeled-robot is required to track

https://doi.org/10.1017/S0263574712000124 Published online by Cambridge University Press

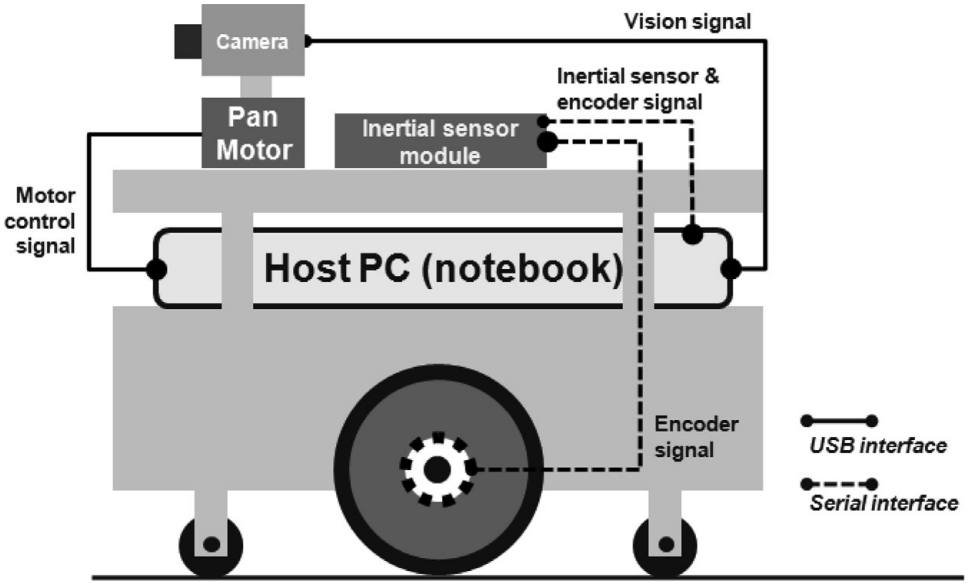


Fig. 9. Schematic diagram of hardware configuration.

the target. The mono camera (SPC 520NC, Phlips) and DC motor (1512SR_IE2–16, Faulhaber, Gmbh & Co. KG) are implemented for the actuation module. The resolution and the frame rate of camera are set to 320 × 240 pixels and 10 fps to achieve ideal processing of the image. The vision-based tracking system usually required about a 30 fps input rate for the vision information[5,6] However, the proposed vision tracking system needs less than 10 fps vision information. Because the proposed system mainly depends on the robot position information, and the vision information

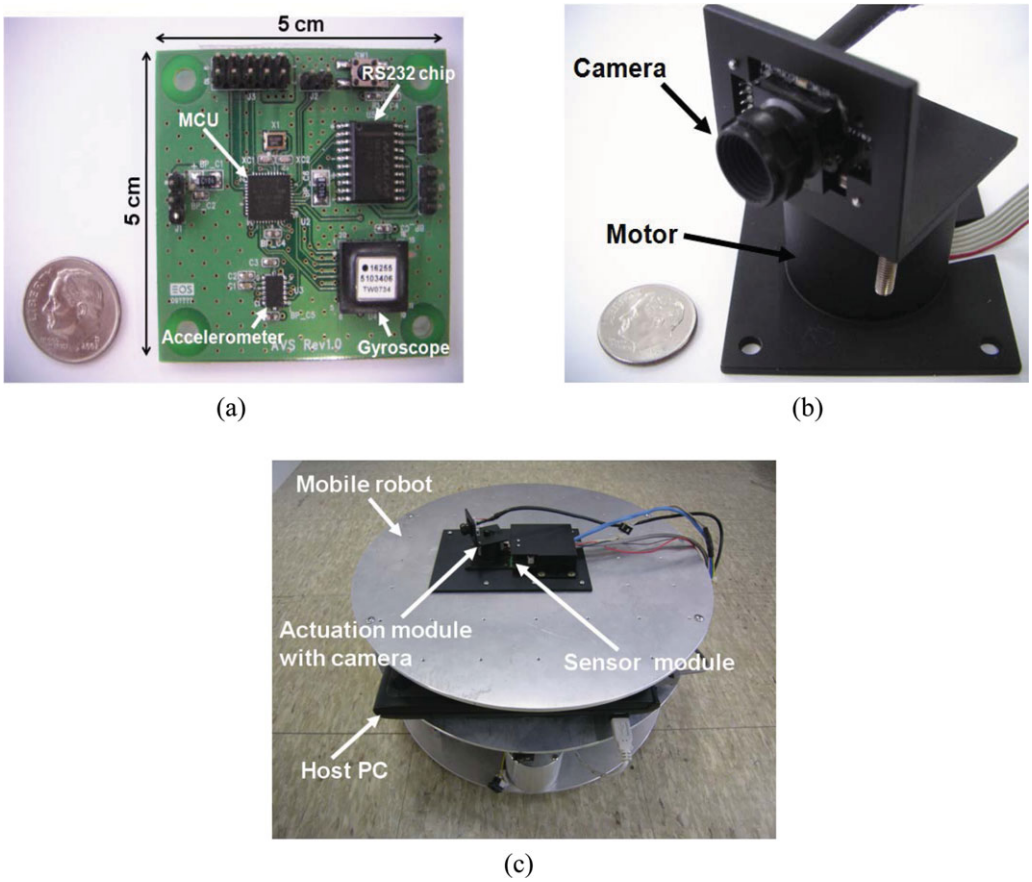


Fig. 10. (Colour online) Picture of developed sensor module, actuation module with the camera, and vision tracking system mounted on the mobile robot. (a) Picture of the developed sensor module. (b) Picture of the developed pan motion actuation module with the camera. (c) Developed line of sight control system mounted on the mobile robot.

https://doi.org/10.1017/S0263574712000124 Published online by Cambridge University Press

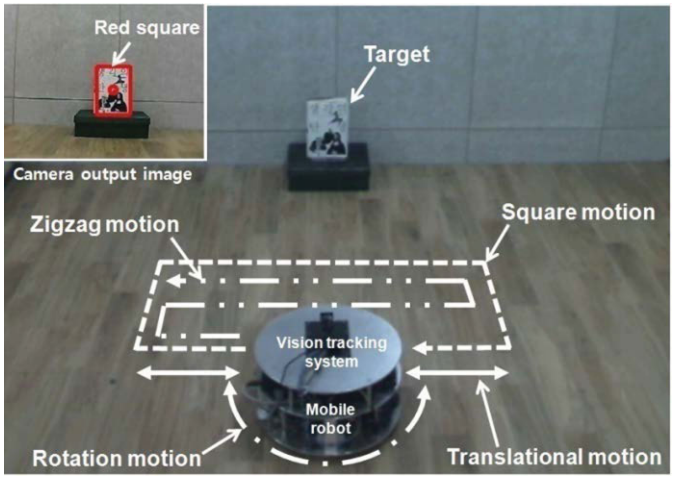


Fig. 11. (Colour online) Picture of experimental environment setup with robot trajectories.

is used as supplementary information. As shown in Fig. 10(c), the developed systems are implemented on a two-wheeled robot (Mobile Robot, Customer & Robot Co., Ltd.). The host computer is mounted on the mobile robot platform. Overall software program is designed for controlling the robot and the DC motor using C++, which is based on the Microsoft Windows environment.

8. Experimental Results

8.1. Experimental results for various motion scenarios

The experimental setup for the developed vision tracking system, which is implemented in the line of sight control system, is shown in Fig. 11. The initial distance between vision system and target is 1.5 m, while driving and rotation velocity of mobile robot are 0.2 m/s and 20 deg/s, respectively. The used motion scenarios are linear motion, rotational motion, square motions with and without the wheel-slip, and zigzag motions with and without the wheel-slip. The SURF based recognition program is used in the recognition performance test. A red square is formed on the edge of the target in the case of recognition success, as shown in Fig. 11. The tracking success rate and recognition rate of the developed system are tested for various robot trajectories. In addition, a pixel error is measured to verify the tracking accuracy. The pixel error denotes the moving pixel quantity of the target image in the image frame. Thus, the smaller pixel error implies better tracking performance.

In the experimental results for the nonslip condition, tracking success rate is 100% in all cases, while recognition rate is 100%, except for the results of the square motion and the zigzag motion. The target cannot be recognized successfully in some output images of these two robot motions due to the blurring effect in image plane. The measured average pixel error is less than 21 pixels. The position estimation results of the disturbance compensator for the square and zigzag motions are illustrated in Fig. 12. The estimated robot positions are accurately for both motions. The experimental results for various robot trajectories are summarized in Table I.

Tracking performance in the slip case is experimented for the square motion and zigzag motion. The specific robot trajectories for the slip case are shown in Fig. 13. The barrier in the ground blocks the moving robot, and wheel-slip occurred for a moment. The driving speed and rotation speed are the same as previous experiments. First, the performance of the slip detector is verified. The result of the slip detector for the square motion with the wheel-slip condition is shown in Fig. 14. In Fig. 14(a), the difference between the two velocity estimations is relatively high

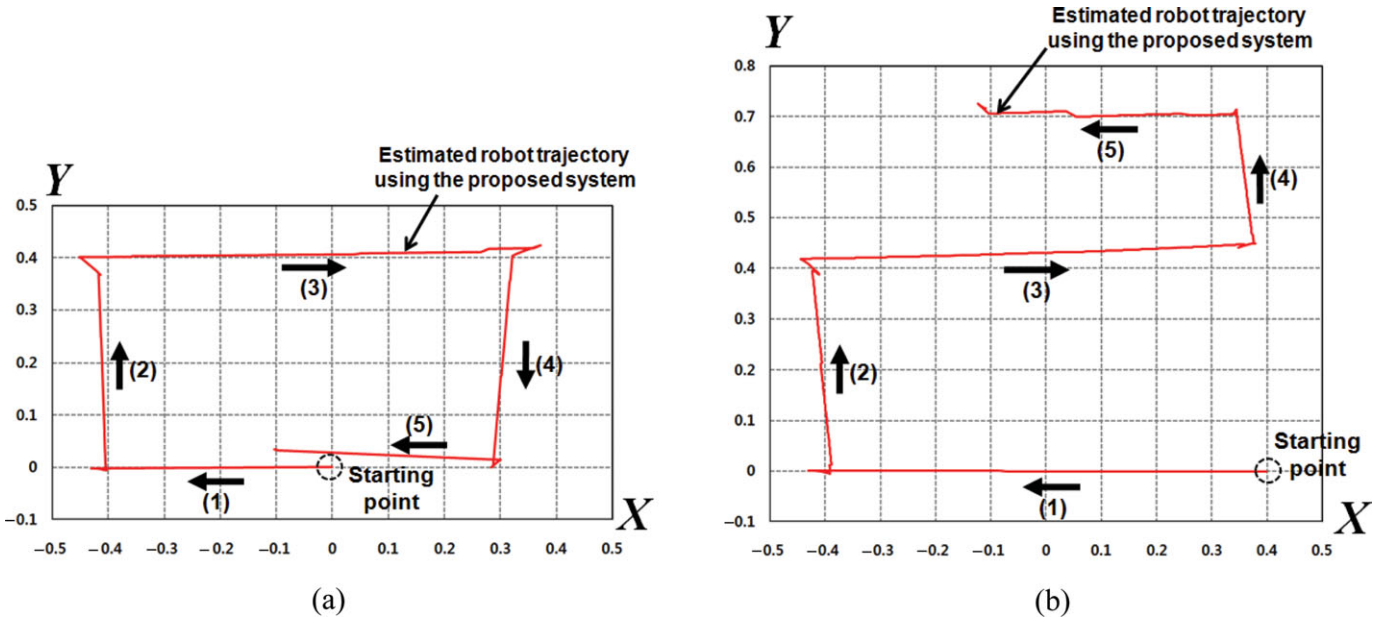


Fig. 12. (Colour online) Estimated robot trajectories for the square motion and zigzag motion without slip conditions. (a) Estimated robot trajectory for the square motion without slip occurrence. (b) Estimated robot trajectory for the zigzag motion without slip occurrence.

https://doi.org/10.1017/S0263574712000124 Published online by Cambridge University Press

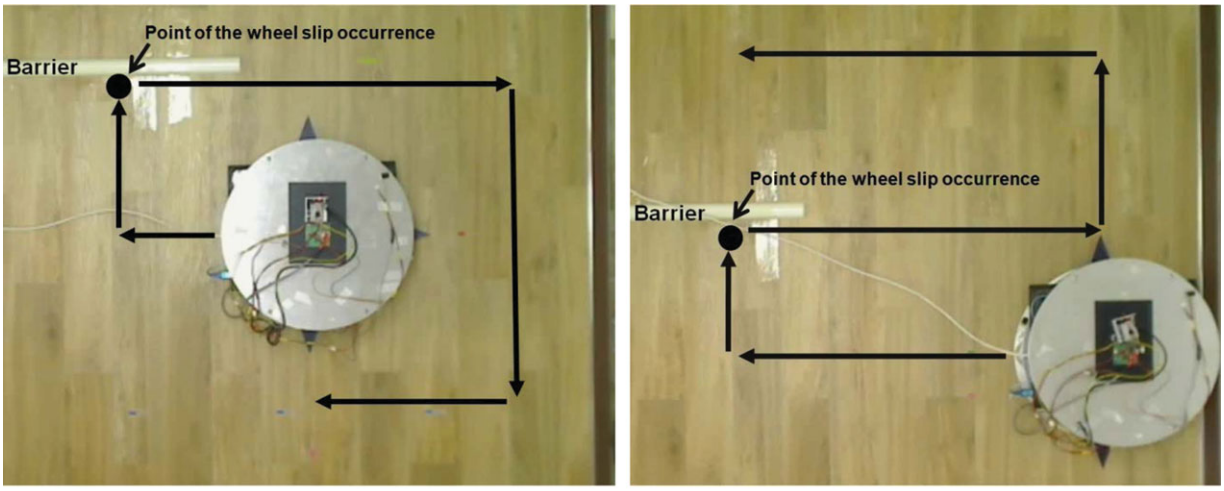


Fig. 13. (Colour online) Robot trajectories for the slip case. (a) Square robot motion with the slip condition. (b) Zigzag robot motion with the slip condition.

in the second peak, where wheel-slip occurs. This is shown clearly in Fig. 14(b) which shows the difference between velocity estimations. At 17 s, the difference is higher than the threshold of the slip detector. Estimated robot position using the disturbance compensator is shown in Fig. 15. The actuators of robot wheels are actuated according to the robot motion commands. The wheel-encoder data show the information of the robot actuators. Thus, the estimated robot position based on the wheel-encoder data is the input trajectory. The real trajectory of the robot is computed from movie clips. The robot trajectories of the three cases are similar before the slip occurrence point under square motion with the slip condition. However, the estimated trajectory from the wheel-encoder is unable to trace the real trajectory after the slip occurrence. In contrast, the error between the estimated trajectory from the developed system and the real trajectory is less than 0.12 m after the slip. For the zigzag motion with the slip condition, the experimental result is similar to the case for square motion. The difference between the estimated robot trajectory using the encoder data and real trajectory increases after the slip. However, the estimated error of the developed system is less than 0.06 m, even after the wheel-slip. The estimation error of the developed system is mainly due to the bias error of the accelerometer data in the rotational motion. The tracking success rate is 100% in both cases in the tracking performance tests for slip case. The recognition rate of the square motion and the zigzag motion with the slip condition is 90.5% and 91.0%. The average pixel error is about 21 pixels. The recognition rate is decreased and the pixel error is increased compared to the nonslip case. This reduction in tracking performance is due to the impact of the collision. The experimental results for the slip case are summarized in Table II. All of the presented results in Table I and Table II are the average of five experiments.

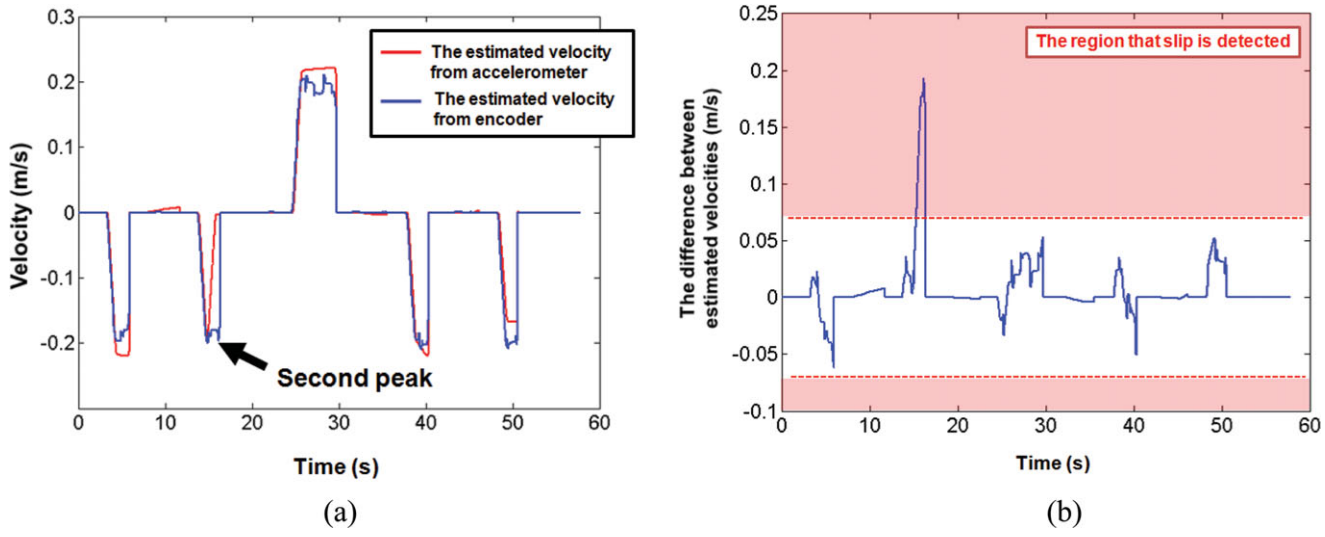


Fig. 14. (Colour online) Estimated velocities from accelerometer and encoder, and the difference between estimated velocities. (a) Estimated velocities from accelerometer and encoder for square robot motion. (b) Difference between estimated velocities using accelerometer and encoder.

https://doi.org/10.1017/S0263574712000124 Published online by Cambridge University Press

Table I. Summary of experimental results for various robot trajectories without the wheel slip condition.

Robot trajectory	Tracking success rate*	Recognition rate**	Pixel error (RMS)
Linear motion	100% (129/129)	100% (129/129)	7.6 pixels
Rotational motion	100 % (108/108)	100% (108/108)	16.4 pixels
Square motion	100% (170/170)	91.2% (155/170)	20.8 pixel
Zigzag motion	100% (200/200)	91.4% (182/200)	20.5 pixel

*Number of successful trackings/Number of total image frames.
**Number of successful recognitions/ Number of total image frames.

Table II. Summary of experimental results for robot trajectories with the wheel slip condition.

Robot trajectory	Tracking success rate	Recognition rate	Pixel error
Square motion with slip	100%	90.5%	21.6 pixels
Zigzag motion with slip	100%	91.0%	21.0 pixels

8.2. Comparison of vision-based system and developed system

To verify robustness of the developed vision tracking system to various circumstances, we performed experiments for two cases. In the experiments, the robot motion is square motion with a driving velocity of 0.2 m/s, and rotation velocity of 20 deg/s. The vision-based tracking system is developed using the SURF algorithm and pin-hole camera model, as mentioned in Section 3.2, to compare the tracking performance of the developed vision tracking system and vision-based tracking system. First, the tracking success rate is tested when an obstacle temporarily blocks the camera sight. As shown in Fig. 16(b), complete vision information is not produced due to poor recognition results. In this case, the vision-based tracking system cannot track the target with this deficiency in vision information. However, using the robot position information of the robot, the developed

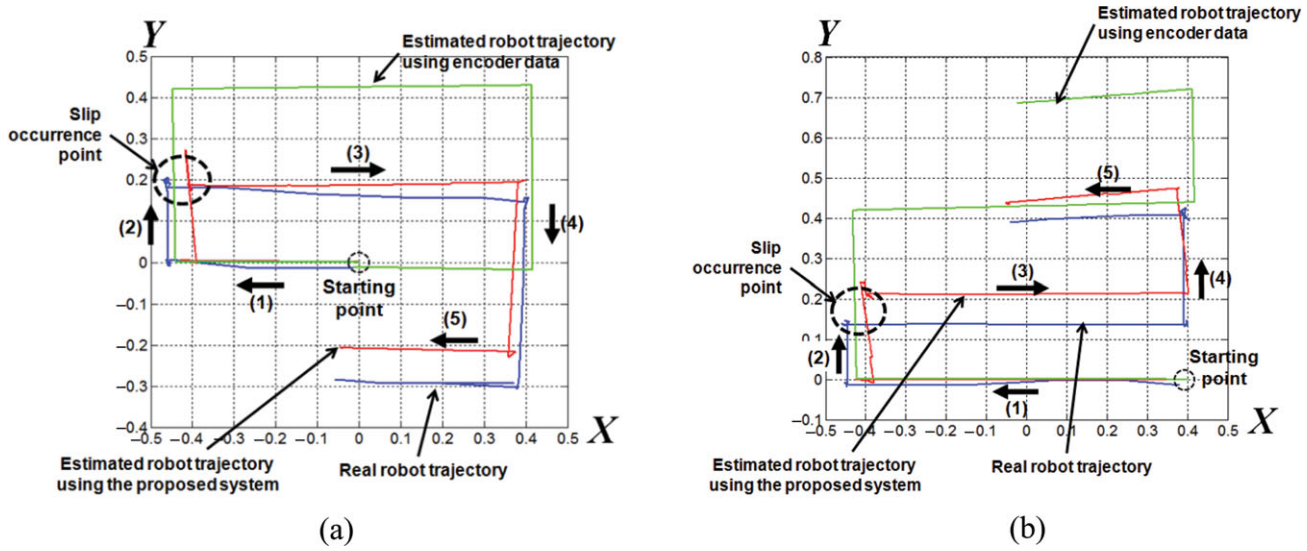


Fig. 15. (Colour online) Estimated robot trajectories from the slip disturbance compensator for wheel-slip cases. (a) Robot trajectory comparison for the square motion with slip occurrence. (b) Robot trajectory comparison for the zigzag motion with slip occurrence.

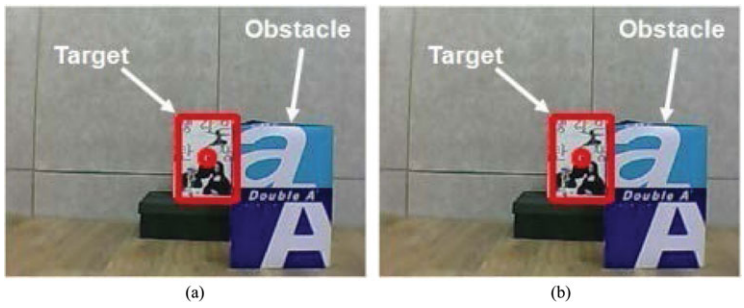


Fig. 16. (Colour online) Output images of camera with obstacle. (a) Obstacle blocks the target (perfect red square is formed). (b) Obstacle blocks the target mostly (red square is not formed).

https://doi.org/10.1017/S0263574712000124 Published online by Cambridge University Press

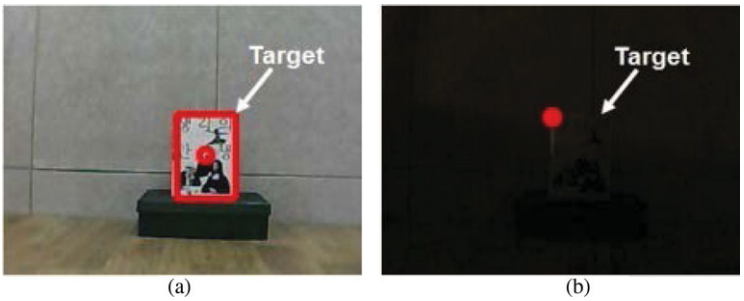


Fig. 17. (Colour online) Output images of camera with illumination change. (a) Outside light on (perfect red square is formed). (b) Outside light off (red square is not formed).

Table III. Summary of experimental results for tracking test with the obstacle and illumination change.

Circumstance	Vision tracking system	Tracking success rate
Obstacle blocks target	Proposed system	100% (175/175)
	Vision-based tracking system	33% (57/175)
Outside illumination change	Proposed system	100% (172/172)
	Vision-based tracking system	37% (63/172)

system fixes the camera sight to the target, while the target is temporarily blocked by the obstacle. The target is tracked and recognized continuously after the obstacle is removed. In the experimental results, the tracking success rate of the developed system is 100% for the square motion. In the second place, the tracking success rate is tested when outside illumination changes while the robot is moving. The target is recognized easily in the normal lighting condition but it does not appear clearly in the image frame when illumination is lowered, as shown in Fig. 17(b). In these cases, either unstable vision information is produced from the recognition results, or the vision information is not produced at all. Therefore, the vision-based tracking system cannot track the target in the absence of normal visual information. However, in spite of the illumination change, the developed vision tracking system can track the target continuously using the estimated robot position information. In the experimental results, the tracking success rate of the developed system is 100% while the outside illumination is changed occasionally during the square motion of the robot. In both cases, the vision-based tracking system is unable to perform the tracking function after the target is blocked by obstacles or illumination is changed. Therefore, the tracking success rates of the vision-based tracking system decline remarkably. The experimental results for various circumstances are summarized in Table III. All the presented results are the average of five experiments, as in the previous experimental results.

9. Conclusions

This paper presents the development of a novel line of sight control system for a robot vision tracking system using vision feedback and position feedforward. The proposed system uses the estimated robot position information relative to the target, which is computed using the inertial sensors and the wheel-encoders data, to improve the performance in vision tracking system. To implement the system, the disturbance compensator is developed to determine the current position of the robot even when the robot wheels slip. The disturbance compensator consists of two EKFs and a slip detector. One Kalman filter based on the gyroscope and wheel-encoders data handle the nonslip case. The other Kalman filter based on the accelerometer and gyroscope data handles cases in which slip is incurred. Each Kalman filter uses a different sensor combination to estimate the robot motion. Accurate robot position and motion are estimated, even when the robot wheels slip, using this combination. The vision feedback information is used for the measurement value of each EKF. The final robot position and expected rotation angle of camera are estimated using one of the two filters based on the slip detector output. The developed vision tracking system is mounted on a mobile robot. Tracking success rates, recognition rates, and pixel error are evaluated for various robot trajectories and circumstances. The experiments demonstrate the developed system achieves high tracking and recognition performances under various motion scenarios and circumstances.

Acknowledgments

This work was supported partly by the R & D Program of the Korea Ministry of Knowledge and Economy (MKE) and the Korea Evaluation Institute of Industrial Technology (KEIT) [2008-F-037-01, Development of HRI Solutions and Core Chipsets for u-Robot].

References

1. M. Lenderman, *Experience the Message: How Experiential Marketing Is Changing the Brand World* (Carroll & Graf Publishers, New York, 2006).
2. D. Kragić and M. Vincze, "Vision for robotics," *Found. Trends Robot.* **1**(1), 1–78 (2010).
3. S. Nadimi and B. Bhanu, "Multistrategy Fusion Using Mixture Model for Moving Object Detection," *Proceedings of the International Conference on Multisensor Fusion and Integration for Intelligent Systems 2001*, Germany (Aug. 20–22, 2001) pp. 317–322.
4. Z. Jia, A. Balasuriya and S. Challa, "Vision based target tracking for autonomous land vehicle navigation: A brief survey," *Recent Patents Comput. Sci.* **2**, 32–42 (2009).

https://doi.org/10.1017/S0263574712000124 Published online by Cambridge University Press

5. N. Pinto, D. D. Cox and J. J. DiCarlo, "Why is real-world visual object recognition hard?," *PLoS Comp. Bio.* **4**(1), 151–156 (2004).
6. D. Kragić and H. H. Christensen, "Cue integration for visual servoing," *IEEE Trans. Robot. Autom.* **17**(1), 18–27 (2001).
7. Y. Cai, N. de Freitas and J. J. Little, "Robust Visual Tracking for Multiple Targets," *Proceedings of the European Conference Computer Vision*, Austria (May 7–13, 2006) pp. 107–118.
8. P. Nillius, J. Sullivan and S. Carlsson, "Multi-Target Tracking - Linking Identities Using Baysian Network Inference," *Proceedings of the 2006 IEEE Computer Vision and Pattern Recognition (CVPR 2006)*, Wasington, DC (Jun. 17–22, 2006) pp. 2187–2194.
9. B. Jung and G. S. Sukhatme, "Real-time motion tracking from a mobile robot," *Int. J. Soc. Robot.*, **2**(1), 63–78 (2010).
10. M. Dai, T. Raphan and B. Cohen, "Adaptation of the angular vestibulo-ocular reflex to head movements in rotating frames of reference," *Exp. Brain Res.* **195**(4), 553–567 (2009).
11. M. Hwangbo, J.-S. Kim and T. Kanade, "Inertial-Aided KLT Feature Tracking for a Moving Camera," *Proceedings of the 2009 IEEE/RSJ International Conference Intelligent Robots and Systems*, St. Louis, MO (Oct. 10–15, 2009) pp. 1909–1916.
12. Z. Jia, A. Balasuriya and S. Challa, "Sensor fusion-based visual target tracking for autonomous vehicles with the out-of-sequence measurements solution," *Robot. Auton. Syst.* **56**(2), 57–176 (2006).
13. M. Ribo, M. Bradner and A. Pinz, "A flexible software architecture for hybrid tracking," *J. Robot. Syst.* **21**(2), 53–63 (2004).
14. D. Xu and Y. F. Li, "A New Pose Estimation Method based on Inertial and Visual Sensors for Autonomous Robots," *Proceedings of the IEEE International Conference on Robotics and Biomimetics*, Sanya, China (Dec. 15–18, 2007) pp. 405–410.
15. L. Lobo and J. Dias, "Inertial sensed ego-motion for 3D vision," *J. Robot. Syst.*, **21**(1), 3–12 (2004).
16. T. Shibata and S. Schaal, "Biomimetic gaze stabilization based on feedback-error-learning with nonparametric regression networks," *Neural Netw.* **14**, 201–216 (2007).
17. S. Xie, J. Luo, Z. Gong, W. Ding, H. Zou and X. Fu, "Biomimetic Control of Pan-tilt-zoom Camera for Visual Tracking Based-on an Autonomous Helicopter," *Proceedings of the 2007 IEEE/RSJ International Conference Intelligent Robots and Systems*, San Diego, CA (Oct. 29 – Nov. 2, 2007) pp. 2138–2143.
18. A. Lenz, T. Balakrishnan, A. G. Pipe and C. Melhuish, "An adaptive gaze stabilization controller inspired by the vestibulo-ocular reflex," *Bioinsp. Biomim.* **3**, 1–11 (2008).
19. H. K. Ouh, W. Bahn, J. Park, W. S. Hwang, H. I. Kwon, K. S. Kim and D. I. Cho, "VOR Based Target Tracking System with an Accelerometer for Mobile Robots," *Proceedings of the 6th International Conferenceon Ubiquitous Robots and Ambient Intelligence*, Gwangju, Korea (Oct. 28–31, 2009) pp. 133–137.
20. N. Dieringer, "Vestibular system," **In**: *Encyclopedia of Life Sciences* (John Wiley & Sons, Hoboken, NJ, 2006).
21. J. S. Lim, T. H. Lee, T. D. Ahn, K. H. Yoo, A. R. Lee and D. I. Cho, "Sensor Fusion for Mobile Robot Navigation Using Accelerometers and Odometer," *Proceedings of the 13th International Conferenceon Advanced Robotics*, Jeju, Korea (Aug. 21–24, 2007) pp. 343–348.
22. R. Mazl and L. Preucil, "Vehicle localization using inertial sensors and GPS," *Springer Tracts Adv. Robot.* **24**, 135–144 (2006).
23. A, V. Oppenheim and R. W. Schafer, *Discrete-Time Signal Processing*, 3rd Ed. (Pearson Prentice Hall, Upper Saddle River, NJ, 2010).
24. R. Y. Tsai, "A versatile camera calibration technique for high accuracy 3D machine vision metrology using off-the-shelf TV cameras lenses," *IEEE Trans. Robot. Autom.* **3**(2), 323–344 (1987).
25. H. Bay, T. Tuytelaars and L. V. Gool, "Speeded-up robust features (SURF)," *Comput. Vis. Image Underst.* **110**(3), 346–359 (2008).
26. A. Alessandri, G. Bartolini, P. Pavanati, E. Punta and A. Vinci, "An Application of the Extended Kalman Filter for Integrated Navigation in Mobile Robotics," *Proceedings of the American Control Conference 1997*, Albuquerque, NM, (Jun. 4–6, 1997) pp. 527–531.
27. J. Park, W. Hwang, H. Kwon, J. Kim, C. Lee, M. L. Anjum, K. Kim and D. Cho, "High Performance Vision Tracking System for Mobile Robot Using Sensor Data Fusion with Kalman Filter," *Proceedings of the 2010 IEEE/RSJ International Conference on Intelligent Robots and Systems*, Taipei, Taiwan (Oct. 18–22, 2010), pp. 3778–3783.
28. L. Ojeda, G. Reina, D. Cruz and J. Borenstein, "The FLEXnav precision dead-reckoning system," *Int. J. Veh. Auton. Syst.* **4**(2–4), 173–195 (2008).
29. D. Simon, *Optimal State Estimation: Kalman, H Infinity, and Nonlinear Approaches* (John Wiley & Sons, Hoboken, NJ, 2006).
30. L. Armesto, J. Tornero and M. Vincze, "On multi-rate fusion for non-linear sampled-data systems: Application to a 6D tracking system," *Robot. Auton. Syst.* **56**(8), 706–715 (2008).
31. L. Ojeda, G. Reina and J. Borenstein, "Experimental Results from FLEXnav: An Expert Rule-Based Dead-Reckoning System for Mars Rovers," *Proceedings of the 2004 IEEE Aerospace Conference*, Big Sky, MT, USA (Mar. 6–13, 2004) pp. 816–825.
32. A. I. Mourikis, S. I. Roumeliotis and J. W. Burdick, "SC-KF mobile robot localization: a stochastic cloning kalman filter for processing relative-state measurements," *IEEE Trans. Robot.* **52**(10), 1813–1825 (2007).
33. M. Seyr and S. Jakubek, "Proprioceptive Navigation, Slip Estimation and Slip Control for Autonomous Wheeled Mobile Robots," *Proceedings of the 2006 IEEE International Conference on Robotics, Automation and Mechatronics*, Bangkok, Thailand (Jun. 7–9, 2006) pp. 1–6.

https://doi.org/10.1017/S0263574712000124 Published online by Cambridge University Press